

Melamine Faced Panel Inspection, Towards an Efficient Use of Natural Resources

Fernando P. G. de Sá¹, Cristhian Aguilera², Cristhian A. Aguilera³, and Aura Conci¹

Abstract Today an adequate use of natural resources respecting the extraction, transformation, and consumption limits considering that we live in an already saturated planet is paramount. The growing environmental consciousness inserted in the new economy encourages the industry to adopt new technologies in order to optimize production processes. The timber industry deals with a feed-stock sensitive to environmental appeals, which demand tight control over the origin of the processed wood. The adoption of automatic and non-destructive techniques to find defects in wood products improve the use of several natural resources such as soil, water, and others environmental provisions. In this work, we present a new image processing technique for quality control tasks of medium density fiber (MDF) and high-density fiber (HDF) melamine boards. This only uses information from one channel acquired in the near-infrared spectrum. We carry out a classification study of defects present in the manufacture of melamine boards. We consider the most important type of defects: stains, paper (displacement or) detachment, (paper crap or) attached material, wrinkled paper, and folded paper. Each group of defects presents different cardinalities, demanding a number of considerations for set normalization and definition of proper techniques for data adjustments in the data mining process of unbalanced sets. The results outperform the literature's previous work on the classification of defects on analysis of the same type of boards.

Keywords: Surface fault detection, near-infrared images, melamine faced panels.

Fernando P. G. de Sá and Aura Conci
Institute of Computing - IC, Federal Fluminense University, Gal. Milton Tavares de Souza s/n, Niterói, 24210-310 (Rio de Janeiro - RJ), Brazil, e-mail: {fernandosa, aconci}@id.uff.br
<http://www.ic.uff.br/>

Cristhian Aguilera
Department of Electrical and Electronics Engineering, University of Bío-Bío, Collao 1202, Concepción, 4051381, Chile, e-mail: cristhia@ubiobio.cl <http://www.biobio.cl/>

Cristhian A. Aguilera
Departamento de Ciencias de la Ingeniería, University of Lagos, Av. Fuchslocher 1305, Osorno, 5290000, Chile, e-mail: cristhian.aguilera@ulagos.cl <http://www.ulagos.cl/>

1 Introduction

The best use of wood and the manufacture of defect-free boards for the construction and furniture industry are key elements for the manufacture of homes and furniture in an environment-friendly environment in modern cities. In recent years, the manufacture of boards for use in the creation of modern spaces in cities has undergone a significant change from the point of view of new designs and materials. These new designs and materials bring new challenges in terms of use and final quality. In the case of melamine boards, boards built on the basis of wood covered by melamine sheets, quality control is a critical task that requires an increasingly intelligent inspection system to identify defects in boards with increasingly more designs. Complex advances in technology (particularly in the field of Industry 4.0) enable the generation and integration of increasingly intelligent systems that are consistent with production processes. Final products without defects, compliance with regulations, and quality standards do not only affect the productivity rates of companies but also play a notable role in the positioning of companies in the market, due to the consequent rejection reductions and especially in customer loyalty increase.

The wood industry has significant global growth and a high projection, despite the global pandemic, for the coming years. The wood-based panel market was estimated at over 1000 million cubic meters in 2021, and the market is projected to register a CAGR (Compound Annual Growth Rate) of over 6% during the forecast period (2021-2026), according to Mordor Intelligence (<https://www.mordorintelligence.com/industry-reports/wood-based-panel-market>). This increase also includes different types of products such as: boards for the construction industry; medium density fiberboard (MDF); high-density fiberboards (HDF); oriented strand board (OSB) and melamine boards. These new products are also characterized by new designs, beyond whiteboards or solid colors, generating boards with complex multicolored designs that make it increasingly difficult to detect defects.

The detection and classification of superficial defects, particularly in melamine boards, is one of the most important tasks in the quality control phase of manufacturing companies. Since it allows generating and evaluating statistics that help to correct possible failures and errors in the manufacturing process that cause faults and also allows the panels to be classified into various classes according to the destination market.

Different defects may appear in the board manufacturing process, such as stains, scratches, material detachment, paper slippage, stuck paper, glued paper among many others. Some of those defects, such as stains, for example, are very common in wood products, but others, such as glued paper, are more complex to identify, mainly when aspects such as light reflection, low-contrast surfaces, complex designs, small defect sizes, among others, are present in the production process [1].

Defects result in laminate wood products with different qualities and consequently marked valor (and prices). In the commerce of objects made of them, it is necessary to identify what type the fault could be present in it, to guarantee: (1) better use of natural resources in the laminate wood industry, (2) the correct pricing and (3)

adequate quality information to the customers. Moreover, identifying a type of defect sometimes can be very difficult, because some of them are similar to human eyes and needs huge attention of experts. Due to this a number of imaging have been used to help with defect identification by using computer vision and pattern recognition techniques. Techniques like x-ray scanning, visible light optical acquisitions (by RGB cameras), ultrasound, microwave sensors, terahertz scanners, and even moisture of separated parts of the electromagnetic spectrum have been investigated in terms of possibilities to provide complementary information for the wood processing industry because each one presents advantages and difficulties on these tasks.

In this work, an exploratory study is presented for the classification of defects in melamine boards using the Near-Infrared Images (NIR) wavelength. The used data-set was obtained in an industrial production line of melamine boards, by means of an array of multiple cameras, capable of taking information in real-time from boards. In this development, a total of 2,778 different samples of infrared images, each one stored in Portable Network Graphics (PNG) format are used. The complete labeled data available consists of 1,919 samples for training, 572 for validation, and 287 for test, all from 5 types of surface defects and a group of perfect boards. The data set was obtained under normal operating conditions of the plant, generating an unbalanced data set naturally related to the frequency of occurrence of defects in the industry on observation [1].

As main characteristics of melamine panel, we can highlight it is a board made of chipboard particles, covered with a sheet of melamine resin named *paper* in this industrial plant. The board is composed of small fragments of pinewood, usually called pine chips, pressed and selected to later be mixed with special adhesives; generally based on water, resin, and chemical hardeners. After the mixture is ready, the particleboard and the sheet are fused together using a heating and pressing system, thus completing the manufacture of the board.

In the board manufacturing process, faults can occur in each of the production stages and they can be reflected in the final quality of the board at the end of the production line. A critical aspect in the quality of the boards is the appearance of stains or foreign objects on the board that alters its visual and aesthetic condition, a factor that is very sensitive for end customers. Another common problem or defect that appears in the production process is the sliding of the melamine thin plate on the board (*paper*). Although this mistake may not be critical (depending on the displacement), it is difficult to detect by manual and automatic inspection systems.

On the manufacturing processes considered here and for this work analysis, five common surface defects are important to be distinguished in the fusion of the sheet and the board: detachment of material, stained paper, smeared paper, broken paper and glued paper.

In figure 1 we can see the appearance as NIR images for these different types of defects in melamine boards: a) Normal is a board without defect; b) Detachment of material, occurs when the board is damaged and has some exposed parts without melamine laminate; c) Stained or smudged paper, appears when stains appear on the final product, due to poor handling of the sheet or the presence of dust and suspended particles; d) Displaced or wrinkled paper, it appears when an unwanted displacement

or wrinkle of the sheet occurs, preventing the board from being completely covered; e) Paper broken (or folded), appears when the sheet breaks (or folds) and part of the board are exposed; and f) Attached or pasted paper appears when an unwanted piece of sheet appears below the melamine thin plate to be glued. Such a description of the defect is very important because their names could vary among the different plants, inspection organizations, or institutions. However, the defects described above represent more than 97% of defective boards in production. This is why the timely detection and classification of those defects is crucial for the commercialization of boards in the international market.

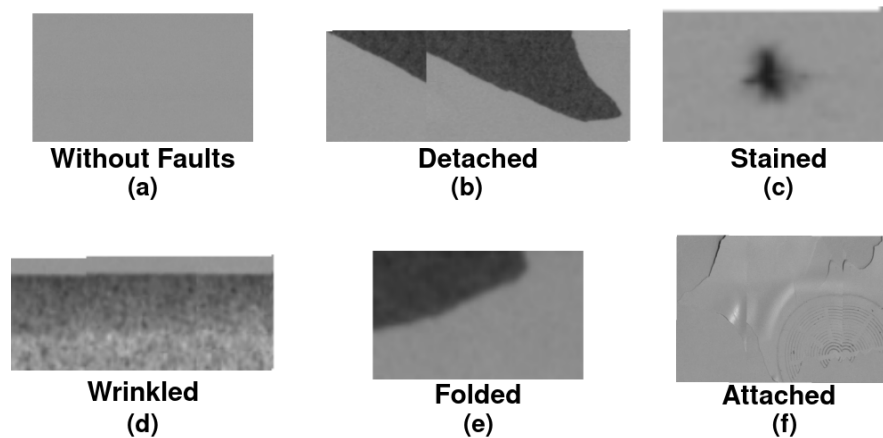


Fig. 1 NIR appearance of the types of defect on melamine board surfaces considered in this work.

2 Related Works

The rapid development of artificial intelligence technology has led to its increasing application in different fields. The use of computer-aided diagnosis employing data driven techniques was subject of recent works for wood defect detection. In these works one remarkable element is the adoption of nondestructive testing of wood to reach economic and sustainability requirements. Luckily, a wide variety of inspection techniques meet these requirements, including laser testing, acoustic-emission technology, computer tomography, high-speed camera, among others. In general, the application of these techniques generates an amount of data which are later processed to find worthy insights.

For example, in computer vision-related works using data from images taken by visible-light (RGB) cameras, we found in the literature the use of the gray-level co-occurrence matrix (GLCM) method for segmentation and classification of knots on wooden surfaces [2]. Tamura *et al.* [3] presented a system based on

texture parameters. In another work presented by Yuce *et al.* [4], the aforementioned approach is adopted to classify different types of defects in wood plates using artificial neural networks (ANN).

Others authors used the support vector machine (SVM) classification algorithm in their works [5] combined with different feature extraction methods. Mahram *et al.* [6] focused on the intensity and the size of different types of knots on wooden surfaces. Cover & Hart [7] developed an approach merging texture descriptors and K-nearest neighbor (KNN) in addition to SVM [8].

Brahnam *et al.* [9] proposed a method of detection and classification of knots and cracks using local binary patterns (LBP) as feature descriptors [9]. Prasitmeeboon & Yau [10] analyze bivariate histograms and Nurthohari *et al.* [11] use the histogram of oriented gradients (HOG) as feature vectors in their analysis. These and other works present different methods to detect common defects on the surface of wood such as knots, cracks, stains or holes [12, 13].

On the other hand, many applications based on image processing have explored the use of information in the near-infrared (NIR) spectrum. This allows obtaining important results because it opens the possibility of processing information that is not available when working only in the visible spectrum (VIS). Semantic segmentation projects, for example, have been presented by Salamati *et al.* [12] and Bigdeli & Süssstrunk [13] using information from the usual R, G, B channels plus the near infrared channel. Works such as those developed by Sharma *et al.* [8], Lee *et al.* [14] and Zhang *et al.* [15] using different algorithms converge in improving images in terms of reducing light influence, perception of details, and texture evaluations.

The detection of defects in production lines has also been favored by contributions that make use of images in the infrared spectrum. For instance, Yean & Kim [16] perform an analysis of the NIR spectrum to detect micro defects in silicon wafers on solar cells (that by the particular nature of the material are very difficult to detect). Hamdi *et al.* [17] propose a system for detecting defects in a production line of textile products by overcoming the lighting disturbances typical of the industrial process. In wood knot detection works, such as the one presented by Hamdi *et al.* [17], the aim is to improve performance indices as in Aguilera *et al.* [1], where a classification system is evaluated through the use of visible and near-infrared images, applying LBP, and using a bag-of-words (BOW) representation and the speed-up robust features (SURF) method for grouping the feature similarity representation.

3 Theoretical Background

From the point of view of algorithms, as seen above, the development of new methods in the area of machine learning has opened the door to new approaches to address the superficial defect detection problem. In this work, we adopt two common approaches of image analysis and multiclass classification processing. The following subsections are dedicated to the theoretical foundation of the used local binary pattern (LBP) and support vector machine (SVM) methods.

3.1 Local Binary Pattern (LBP)

The local binary pattern (LBP) was proposed as a technique for texture representation by [18]. It has a number of variations on the distance from the evaluated pixel neighborhood and directions of computation [19].

The LBP general feature computation generates a code of each pixel considering its values and those of its surroundings using a 2 step algorithm. In the first step of the LBP feature computation, the pixel in analysis for generation the binary code is compared with the neighbor pixels. In case of its value being smaller than those of any neighborhood position, then such a position is set as 1, otherwise as 0. The third image of Figure 2 (top-right) shows an illustration of a Local Binary Pattern.

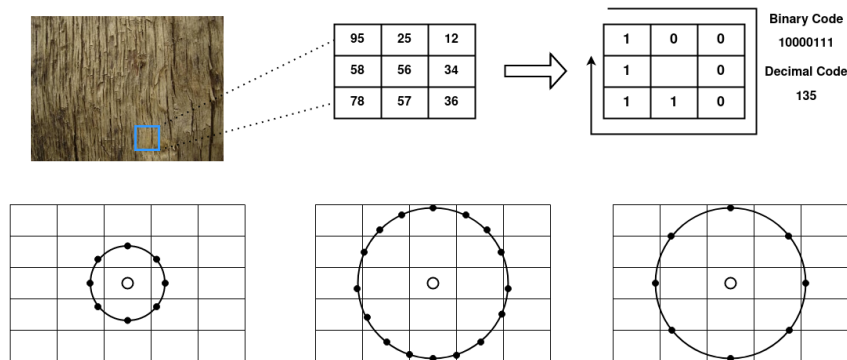


Fig. 2 A neighborhood of an image for distance 1, its gray scale pixel intensities and binary result after comparison between central point and each neighbor (when codification begins in the top left point). Configurations for distance 1 from central pixel and for distance 2 (considering 16 consecutive or 8 alternated values).

In the second step, a binary code is formed considering the set of zeros and ones formed in the first step of the LBP feature computation. This code gives the name to the technique and it is attributed to the central pixel, the named g_0 in Figure 3. However, for each position where the binary number formation begins a different value can be formed. This image shows the binary code and its value (as a decimal number) when the initial position is the top left of the comparison neighborhood achieving: $(1000111)_B = (135)_D$.

Of course even using this clockwise orientation and formation sequence this is only one of 7 other possibilities: $(00001111)_B = (15)_D$; $(00011110)_B = (30)_D$; $(00111100)_B = (60)_D$; $(01111000)_B = (120)_D$; $(11110000)_B = (240)_D$; $(11100001)_B = (225)_D$; and $(11000011)_B = (195)_D$. In other words the 8 bits number formation can begins in any of the $g_1 \dots g_8$ position showed in Figure 3.

Moreover, an anticlockwise orientation (as for instance $g_8, g_7, g_5, g_4, g_3, g_2, g_1$) can be used and other number formation sequence as well (as for instance $g_7, g_6, g_5, g_4, g_8, g_1, g_2, g_3$). Some of such order present special meaning as a

g1	g2	g3
g8	g0	g4
g7	g6	g5

Fig. 3 Reference for the positions at neighborhood 1 to aid on explain the calculation of Equations (1, 2).

representation invariant to reflection or rotations and can be used in order to improve the identification of elements like a constant strap or edge defined by the level or tons.

After the definition of this order, a new position for the set of zeros and ones (of the first step) appears and the named g' representation of Figure 3 is obtained. This new order can be considered in the LBP Equation (1):

$$lbp(g_0) = \sum_{n=1}^{N-1} g'_n 2^{n-1} \quad (1)$$

where $g'_n = \{0, 1\}$, $g'_n = 1$ if the pixel value in position n is greater then the pixel value in g_0 and $g'_n = 0$ otherwise.

There are a number of possible variations related to what can be understood as neighborhood, that is the open or close ball for each point of the image or pixel [20](pp. 102). The Euclidean distance or d_2 is the usual one. This distance in \mathfrak{R}^2 is defined by Equation (2) considering $p=2$. However, for the same pixels organization, other distances can be obtained depending on what is the value of p fixed in the general expression used to compute the distance. p defines in this way d_1 , d_2 and d_∞ , based on Equation (2) [20](pp. 88):

$$d_p(g'_0, g'_n) = (|g'_{0x} - g'_{nx}|^p + |g'_{0y} - g'_{ny}|^p)^{1/p} \quad (2)$$

where $p = \{1, 2, \dots, \infty\}$, x , y are the pixel axial orientation for \mathfrak{R}^2 (that is : $g'_n = (g'_{nx}, g'_{ny})$ and $g'_0 = (g'_{0x}, g'_{0y})$). These x , y coordinates are related to the central point depicted in Figure 4. When $p=2$ it is named Euclidean distance of \mathfrak{R}^2 , the distance from each position g'_n to the central g'_0 are presented in Figure 5. The borders of the neighborhood up to a defined distance have the appearance of circle (Figure 2).

There are other appearances for such balls or neighborhoods depending on the distance function. Figure 6 shows 3 neighborhood appearance for $\rho = \{1, 2, \infty\}$. The numbers present in each position by different colors are the distance computed using Equation (2): from each pixel to the central one. The central image on Figure 6 represents the results using the same distance function of Figure 5 but now with an approximation of 2 decimals only.

Finally, it is important to realize that not all the pixels compounding the ball border up to a given distance need to be used to represent the LBP of an image on

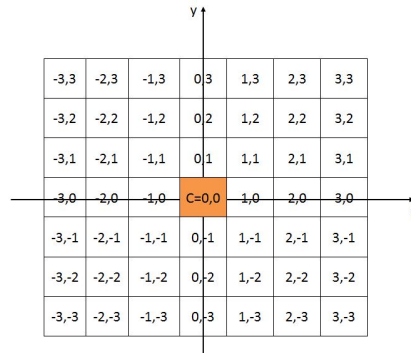


Fig. 4 Coordinates of horizontal and vertical directions 1 and 2 for pixels x, y distance computation.

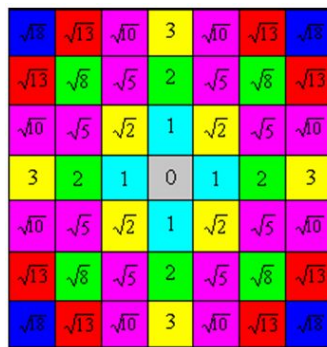


Fig. 5 Equation (2) related to $p=2$ (or Euclidean distance d_2) up 3 neighbors for LBP computation.



Fig. 6 Open ball appearance related to $p=\{1, 2, \infty\}$ on Equation (2) computations, considering neighbourhood of 7 for d_1 and d_∞ .

analysis. For instance for Euclidean distance 2 where a neighborhood of more than 8 pixels around a central one is the usual result (see Figure 2 bottom row) the LBP can be computed using only 8 values, when a number up to 1 byte is enough to store these LBP possible values. However, when greater numbers of 0 and 1 are employed

for the formation of the LBP more bits must be necessary to store this binary number (that will be greater than a value stored in 8 bits, resulting in a need of 2 bytes or more than 3 bytes). That is: in some cases, the maximum number generated for the LBP code can be up to $255 = 2^8 - 1$, or $65,535 = 2^{16} - 1$ or $2^{32} - 1$, and so on. Consequently, depending on the LBP implementation this 1 or 0 can be used up to any number for the composition of a binary number and this can be a parameter to be decided considering the problem under study. The central image in Figure 2 bottom row illustrates the case where 16 is used and, the right image shows the option for the case when only 8 is used, both when Euclidean distance is 2.

3.2 Support Vector Machine (SVM)

Support vector machines are a class of statistical models with extensive use in pattern recognition problems. It attempts to find a suitable hypothesis to the complexity of the training data while minimizing the upper bound of the generalization error [21]. In classification problems, a SVM aims to create a maximum-margin hyperplane to separate the data in distinct classes by choosing a function that transforms the original feature space ensuring the structural risk minimization principle [21].

Let S the training set of features of N classes be represented by a D dimensional feature vector, that is $S = \{(x_n, y_n) \mid x_n \in \mathcal{R}^D, y_n \in \mathbb{Z}, n = 1, \dots, N\}$. By a kernel function ϕ , the input data is projected into a high dimensional feature space to maximize the power of the separating hyperplane. This optimization problem is solved using quadratic programming, whose model is defined below:

$$\begin{aligned} \min_{\mathbf{w}, b} \quad & \frac{1}{2} \|\mathbf{w}\|^2 + C \sum_{n=1}^N \xi_n \\ \text{s.t.} \quad & y_n(\mathbf{w}^T \phi(x_n) + b) \geq 1 - \xi_n, \\ & \xi_n \geq 0, n = 1, \dots, N. \end{aligned} \quad (1)$$

where \mathbf{w} and b are the model parameters, ϕ is kernel function, and C is a hyper-parameter that controls the trade-off between the model complexity and the margin width.

For binary SVM classification, the ground truth labeling is done using $y_n = \pm 1$, with the sign determining if a training instance n is from the positive or the negative class. Once training is complete, the result of Equation (3) induces a straight line separating both classes. Figure 7 shows the maximum hyperplane where $\mathbf{w}x + b = 0$ discriminates the classes as follows: $\mathbf{w}x + b \geq 1$ when $y_n = +1$, and $\mathbf{w}x + b \leq -1$ when $y_n = -1$. Data points over the dotted lines are known as the support vector for satisfying the equality in the equations above. As can be seen in the figure, the slack variables ξ are highlighted to show their values when violated.

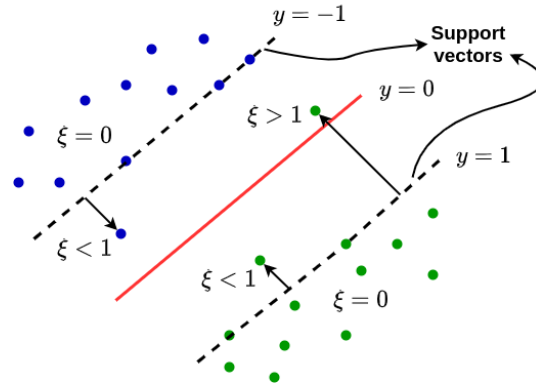


Fig. 7 Geometric representation of SVM: a red hyperplane discriminates blue and green classes.

Although SVM is inherently a binary classifier, it fashions two possible arrangements in order to support multiclass classification: one-against-one method and one-against-the-rest method [22]. The one-against-one approach is adopted to handle the multiclass classification in our results. The main characteristic of this method is to break down the multiclass problem into multiple binary classification problems. Thus, let m be the number of classes, the one-against-one approach can construct $\frac{m(m-1)}{2}$ hyperplanes respecting the optimized separation between each one of the m classes.

4 Used Methodology for Surface Classification

Before discussing independently each part of the proposed methodology, let us present the general used approach, which consists in feature extraction and classification learning, as presented in Figure 8. It is important to note that in this type of application, i.e. a continuous inspection [23], differently of the usual image processing for object classification there is not the phase of segmentation [24], because there is not objects to be separate of the background in the acquired scene to be analysed.

As can be seen in the Figure 8, from the available data set we extract the features of the gray level counting directly the number of each level present in the images or organizing the level according to their position by using local binary patterns (LBPs). After, these features feed the classification algorithm of support vector machine (SVM) aiming to identify each sample as with or without defects. Finally, numerical indexes are responsible to analyse the quality of the obtained results.

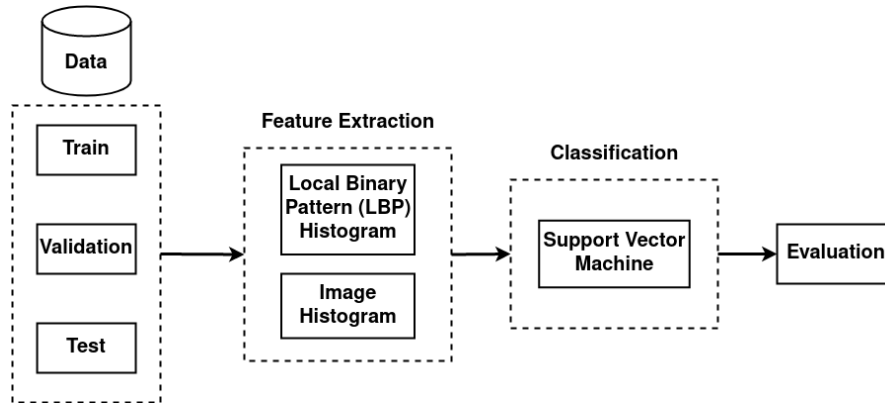


Fig. 8 General approach.

4.1 Used Dataset

Here, the near-infrared spectrum is used because this type of imaging presents advantages on the identification of superficial irregularities [1]. For the image acquisition, a system of multiple cameras and industrial controllers was designed and constructed allowing the simultaneous shooting of each of the cameras to cover a complete board. Such boards have real dimensions of $1.83\text{ m} \times 2.50\text{ m}$. A total of 3 infrared spectrum cameras were used in a melamine panel manufacturing line operating at a speed of 1 m/s . All cameras are connected via a Giga Ethernet network. Basler Aca 1300-60 gmNIR cameras of $1,280 \times 1,024$ pixels were used, generating images of complete boards with a resolution of $3,570 \times 5,770$ pixels [1].

These cameras are used for detection of the most common types of defect found on melamine boards. The NIR information of each board is stored as a single-channel. This channel can be considered as a grey scale image. Some of these are depicted in Figure 1. They are used to compose the classes of the data set, each image having different numbers of pixels. However, their pixels are always described in 256 levels of the channel range. The data set is organized in a way that an image belongs only to one group. That is, the data set presents previous separation for training and validation of the learning phase and then final tests: this structure ensures that there is no sample present at the same time in more than one of these sets. The data set composition can be seen in Table 1.

4.2 Dealing with Imbalanced Data

Correct identification of the types of melamine board superficial issue can be very difficult, because most of the faults present very similar regions over some part of the sample (Figure 1). This is specially complex for the groups of without faults,

Table 1 Original data set composition for all phases.

Classes	Training	Validation	Test	Total
Without Faults	685	249	240	1,174
Detached	122	33	2	158
Stained	246	66	14	326
Wrinkled	587	149	19	755
Attached	157	41	3	201
Folded	124	34	8	164
Total	1,919	572	287	2,778

detached, stained, and folded types of defects. A total of 2,778 NIR spectrum images of melamine panels with defects and without defects were captured, generating a data set with the showed distribution (Table 1).

Once the occurrence of some types of defects is low, the acquired images during the inspection tasks compose a dataset naturally imbalanced, with the predominance of samples from the class ‘without faults’. We adopt a simple under-sampling technique that selects random samples from the m classes to build a new training dataset whose size is limited by the size of minority class [25].

4.3 Used Programming Tools

We use the Python 3.8 computer language and its common libraries are adopted for data manipulation and machine learning development in this work. More specifically the following programming tools are used:

- Image processing: Scikit-image version 0.19.1, OpenCV version 4.5.5
- Machine learning: Scikit-learn version 1.0.2
- Array manipulation: NumPy version 1.22.1

4.4 Features Computation

The general techniques of image analysis can be helpful for the task of features extraction. The proposed approach has two groups of features. The first group represents features related to the pixel intensity and the second group is texture related, that is it considers the pattern distribution of the intensity in a considerable position of a given area (or texel) of each samples.

The Local Binary Pattern (LBP) approach is used for textural evaluation (that is the second group of features). This computation result can be changed by the

selection of the parameters: `method`, `number of points` and `radius` of the used library ¹.

The parameter `radius` define the distance of the considered neighborhood, as represented in Figure 2, top row. The parameter `method` has the options: 'default'; 'ror'; 'uniform' and 'var'. They mean the use of a different organization of the binary number to be created by implementation, they modify the order of the basic algorithm (or 'default'). This is employed in the second step of the LBP computation as explained in section 3.1 and in the used library documentation. The `number of points` corresponds to the maximum possible code to be generated and attributed to the pixel as the LBP code.

After the computation of these features, the number of pixels in each possibility is used to form a histogram of the LBP group that represents the image as a feature vector in the next steps of learning. Figure 9 shows these vectors made of histograms.

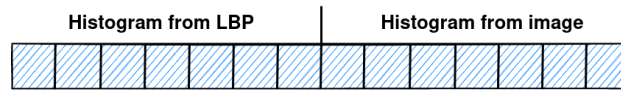


Fig. 9 Histograms compounding the feature vector.

Both LBP and intensity level histograms can present some variations in their computations. The parameters `radius`, `points` and `methods` allow some adjustment in the LBP computations, related to the size of the neighborhood considered and the way the binary number representing the texture is formed, as already mentioned. In this work 8, 13, and 18 are the numbers of bits allowed for the final LBP binary code formation. The used distance was fixed as 3 and 8 (see Figure 2). And the possible methods for organizing the code are considered.

For the intensity level histogram, the number of bins used is a possible variation. The variation of parameters from both histograms as grouped in 8 or 32 bins of division of the maximum values are considered in the classification results to be adjusted by the grid search approach for improving the next classification phase. Figure 9 exemplifies the used vector of features obtained by the histogram combinations. Table 2 shows these possible parameters to be investigates.

4.5 Classification Training and Testing

The next step is learning how to do the classification in each class respectively. An important aspect in this is to choose a classifier that matches better the faults in order it will be used in a future implementation. In this article, the feature vectors are used as input for the Support Vector Machine (SVM) classification algorithm. There are elements for variation in the classification approach the cost functions C , γ and the

¹ https://scikit-image.org/docs/stable/api/skimage.feature.html#skimage.feature.local_binary_pattern

used kernel, these hyper-parameter possibilities are evaluated using Accuracy and F-score.

The fine tuning of SVM and feature parameters is necessary in order to better explore the search space. To accomplish this effort, the Grid Search was employed for an iterative evaluation of the parameters related to the ways the feature vector is built (that is the elements of possible variation in the histograms). The evaluation goes up to the end using the validation to identify the best possible features after training them with some infrared images labeled as with a specific fault type. It is employed in order to evaluate the SVM hyper-parameters to better predict the type of defect from new images in an industrial plant in the future. Figure 10 presents details of in this work adopted strategy to find the best characteristics of the training set.

In the classification step, the validation set has the features used to evaluate the hyper-parameters (cost C , γ and kernel ϕ) according the performed classification. Finally, the test set, which also had its characteristics extracted, is used to evaluate the built model. Processing continues until the entire search space of the grid search has been explored.

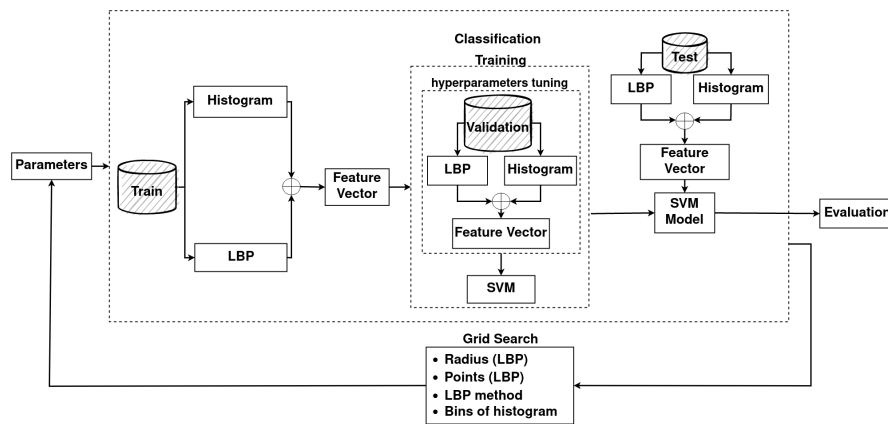


Fig. 10 Adopted processing strategy.

Table 2 presents the search space for grid search parameters and hyper-parameters during the validation processing. Note that the range of the histogram is evaluated only under two settings, 8 to 8 or 32 to 32 levels. Meanwhile, the search space for LBP (radius and number of points and the binary formation) are more extensive.

Table 2 Parameter and hyper parameter search space.

	Parameters/ Hyperparameters	Used values			
Feature Extraction	LBP method	default	ror	uniform	var
	Radius	3		8	
	Number of points	8	13	18	
	Interval of bins	8		32	
Classification	C	1	10	100	120 150
	γ	0.001		0.0001	
	SVM kernel (ϕ)	rbf		linear	polynomial

5 Results

The multi class classification (one vs all) performed by SVM was implemented using the workflow described in Section 4. The purpose of this classification is to distinguish normal samples from those identified as different types of failures, as described in Table 1. The complete exploration of the parameters in the search space was made by grid search and it identified the optimal parameters involved in the feature extraction presented in Table 3. The model validation (after training) determined the optimal SVM hyper parameters described in Table 4.

Table 3 Optimal parameters from feature extraction phase.

Parameters	Value
Radius	28
Number of points	8
Method	default
Bins of histogram	8

Table 4 Optimal hyperparameters from the SVM classifier.

Hyperparameters	Value
C	150
kernel (ϕ)	linear

Table 5 presents the fine-tuned set of parameters and hyper parameters results fitted for each class. The respective averages of Precision, Recall and F-scores obtained in the classification process are presented in Table 6. As you can see, the order from best to worst (or vice versa) varies according to the "metric" used for comparison. For example, for the F-score: normal samples were identified more correctly than any type of defect, reaching a value of 97%, and wrinkled paper is the best identified type of defect (92%). On the opposite side, Detached and Folded faults are the ones with the least satisfactory F-score results. This presents higher values for the class of wrinkled defects and worse for folded papers.

Although, we are collectively calling Accuracy, Precision, Recall and F-scores "metric", note that we are not in fact actually processing them as metric in the metric space sense. Moreover, we are not even concerned that any of them are in fact a metric, or even a semi-metric in a topological space [20]. They are in fact only being here used as a comparative index of performance of the final process, in absence of a more proper international accepted option [26].

Table 5 Resulting multi class confusion matrix.

	Without Faults	Detached	Stained	Wrinkled	Attached	Folded
Without Faults	242	0	1	0	6	0
Detached	0	24	2	2	0	5
Stained	7	0	58	0	1	0
Wrinkled	0	3	12	129	0	5
Attached	2	0	1	0	38	0
Folded	0	3	1	1	0	29

Table 6 Results for each class considering various "metrics".

Class	Precision	Recall	F-score	Overall Accuracy	Macro F-score
Without Faults	0.96	0.97	0.97		
Detached	0.80	0.73	0.76		
Stained	0.77	0.88	0.82	0.91	0.86
Wrinkled	0.98	0.87	0.92		
Attached	0.84	0.93	0.88		
Folded	0.74	0.85	0.79		

6 Comparisons with Previous Work

It is important to evaluate our work in the light of other solutions for the same problem. The work developed by [1] treats similar problem of detection of defects on melamine-faced board. There are three classes of faults equivalent there with the present work. The Table 7 presents these that enable comparison between the two works based on results of classification accuracy of the classes 'Stained', 'Wrinkled' and 'Without Faults'.

Table 7 Comparing average classification considering equivalent classes with previous work.

Classes	Aguilera <i>et al.</i> [1]	Our Work
Stained	0.84	0.96
Wrinkled	0.97	0.96
Without Faults	0.95	0.97

As seen in Table 7, both solutions present equivalent results for 'Wrinkled' and 'Without Faults'. The class 'Stained' presents the higher gain of classification performance using the methodology discussed in this work. Future works can improve the actual results using the approach of feature construction discussed by [27].

7 Conclusion

This work investigates the possibilities of using a single infrared images on the classification of melamine surfaces as with or without defect, considering data set with six (6) possible groups and evaluating 2778 samples of surface, from five (5) types of faults (Table 1). The used data set present originally unbalanced numbers of samples in each type of class. Two types of features are considered in the SVM using grid search and hyper-parameters fine tuning evaluation. In order to train the classifier, the original data set was separated for learning, validation, and test. To promote better balance among classes, each of the classes is adjusted to present the same number of elements where each element has been selected at random.

Comparisons with previous work were investigated. Aguilera *et al.* [1] obtained theirs results after a standardization of the sizes of the analyzed samples and adopting Extended Local Binary Pattern (E-LBP) [28] to extract the features from images. Other details as the SVM model (to perform multi-class classification) used are just like our methodology [1].

Observing Table 7, we can state that the achieved results have been very good, obtaining acceptable degrees of certainty, specially because this is an initial step where there are a lot of possible improvements. These come from reorganizations of the number of samples used in each set of faults and standardization of the sizes of their samples, passing trough the inclusions of other types of feature to be computed and included in the feature vector, other presentation of it to the classifiers (not only histograms) up to more classifiers then only SVM to be included, and even other "metrics" to be tested. All these facts allow the say that NIR presents great possibilities for inspections in this type of continuous classification problem.

Acknowledgements We acknowledge to the CYTED Network "Ibero-American Thematic Network on ICT Applications for Smart Cities", Grant No.: 518RT0559. F.P.G.S. and A.C. express their gratitude to the Brazilian Agencies FAPERJ, CAPES and CNPq.

References

1. Aguilera, C. A., Aguilera, C. & Sappa, A. D. Melamine faced panels defect classification beyond the visible spectrum. *Sensors* **18**, 3644 (2018).

2. YongHua, X. & Jin-Cong, W. Study on the identification of the wood surface defects based on texture features. *Optik-International Journal for Light and Electron Optics* **126**, 2231–2235 (2015).
3. Tamura, H., Mori, S. & Yamawaki, T. Textural features corresponding to visual perception. *IEEE Transactions on Systems, man, and cybernetics* **8**, 460–473 (1978).
4. Yuce, B. *et al.* Neural network design and feature selection using principal component analysis and Taguchi method for identifying wood veneer defects. *Production & Manufacturing Research* **2**, 291–308 (2014).
5. Cortes, C. & Vapnik, V. Support-vector networks. *Machine learning* **20**, 273–297 (1995).
6. Mahram, A., Shayesteh, M. G. & Jafarpour, S. *Classification of wood surface defects with hybrid usage of statistical and textural features in 2012 35th International Conference on Telecommunications and Signal Processing (TSP)* (2012), 749–752.
7. Cover, T. & Hart, P. Nearest neighbor pattern classification. *IEEE transactions on information theory* **13**, 21–27 (1967).
8. Sharma, V., Hardeberg, J. Y. & George, S. RGB-NIR Image Enhancement by Fusing Bilateral and Weighted Least Squares Filters. *Journal of Imaging Science and Technology* **61**, 40409–1 (2017).
9. Brahmam, S., Jain, L. C., Nanni, L., Lumini, A., *et al.* *Local binary patterns: new variants and applications* (Springer, 2014).
10. Prasitmeeboon, P. & Yau, H. *Defect Detection of Particleboards by Visual Analysis and Machine Learning in 2019 5th International Conference on Engineering, Applied Sciences and Technology (ICEAST)* (2019), 1–4.
11. Nurthohari, Z., Murti, M. A. & Setianingsih, C. *Wood quality classification based on texture and fiber pattern recognition using hog feature and svm classifier in 2019 IEEE International Conference on Internet of Things and Intelligence System (IoTIS)* (2019), 123–128.
12. Salamati, N., Larlus, D., Csurka, G. & Süssstrunk, S. *Semantic image segmentation using visible and near-infrared channels in European Conference on Computer Vision* (2012), 461–471.
13. Bigdeli, S. & Süssstrunk, S. *Deep semantic segmentation using NIR as extra physical information in 2019 IEEE International Conference on Image Processing (ICIP)* (2019), 2439–2443.
14. Lee, J., Park, Y. & Jeon, B. *Low intensity rgb texture enhancement based on near infrared image using perceptual information in 2018 10th International Conference on Communications, Circuits and Systems (ICCCAS)* (2018), 422–425.
15. Zhang, X., Sim, T. & Miao, X. *Enhancing photographs with near infra-red images in 2008 IEEE Conference on Computer Vision and Pattern Recognition* (2008), 1–8.
16. Yean, J.-S. & Kim, G.-B. Investigation of laser scattering pattern and defect detection based on Rayleigh criterion for crystalline silicon wafer used in solar

- cell. *Journal of the Korean Society for Precision Engineering* **28**, 606–613 (2011).
17. Hamdi, A. A., Fouad, M. M., Sayed, M. S. & Hadhoud, M. M. *Patterned fabric defect detection system using near infrared imaging in 2017 Eighth International Conference on Intelligent Computing and Information Systems (ICICIS)* (2017), 111–117.
 18. Ojala, T., Pietikainen, M. & Maenpaa, T. Multiresolution grayscale and rotation invariant texture classification with local binary patterns. *IEEE Transactions on pattern analysis and machine intelligence* **24**, 971–987 (2002).
 19. Tan, X. & Triggs, B. Enhanced local texture feature sets for face recognition under difficult lighting conditions. *IEEE transactions on image processing* **19**, 1635–1650 (2010).
 20. Kubrusly, C. S. *The Elements of Operator Theory* 2nd ed. (Birkhauser, 2010).
 21. Vapnik, V. N. The nature of statistical learning. *Theory* (1995).
 22. Weston, J. & Watkins, C. *Multi-class support vector machines* tech. rep. (Cite-seer, 1998).
 23. Conci, A. & Proença, C. A comparison between image-processing approaches to textile inspection. *Journal of the Textile Institute* **91**, 317–323 (2000).
 24. Rodrigues, E., Conci, A. & Liatsis, P. Element: multi-modal retinal vessel segmentation based on a coupled region growing and machine learning approach. *IEEE Journal of Biomedical and Health Informatic* **24**, 3597–3519 (2020).
 25. He, H. & Garcia, E. A. Learning from imbalanced data. *IEEE Transactions on knowledge and data engineering* **21**, 1263–1284 (2009).
 26. Conci, A., Galvão, S. S., Sequeiros, G. O., Saade, D. C. & MacHenry, T. A new measure for comparing biomedical regions of interest in segmentation of digital images. *Discrete Applied Mathematics* **197**. Distance Geometry and Applications, 103–113. ISSN: 0166-218X. <https://www.sciencedirect.com/science/article/pii/S0166218X15002887> (2015).
 27. Zhang, Z. *et al.* From Individual to Whole: Reducing Intra-class Variance by Feature Aggregation. *International Journal of Computing Vision*. <https://doi.org/10.1007/s11263-021-01569-2> (2022).
 28. Liu, L., Zhao, L., Long, Y., Kuang, G. & Fieguth, P. Extended local binary patterns for texture classification. *Image and Vision Computing* **30**, 86–99 (2012).